High-efficiency photon–electron coupling resonant emission in GaN-based microdisks on Si*

Menghan Liu(刘梦涵)[1], Peng Chen(陈鹏)[1,†], Zili Xie(谢自力)[1], Xiangqian Xiu(修向前)[1], Dunjun Chen(陈敦军)[1], Bin Liu(刘斌)[1], Ping Han(韩平)[1], Yi Shi(施毅)[1], Rong Zhang(张荣)[1,‡], Youdou Zheng(郑有炓)[1], Kai Cheng(程凯)[2], and Liyang Zhang(张丽阳)[2]

[1] *Jiangsu Provincial Key Laboratory of Advanced Photonic and Electronic Materials and School of Electronic Science and Engineering, Nanjing University, Nanjing* 210093, *China*

[2] *Enkris Semiconductor Inc. NW-20, Nanopolis Suzhou, 99 Jinji Avenue* 215123, *China*

(Received 29 January 2020; revised manuscript received 13 April 2020; accepted manuscript online 19 May 2020)

Resonance effects caused by the photon–electron interaction are a focus of attention in semiconductor optoelectronics, as they are able to increase the efficiency of emission. GaN-on-silicon microdisks can provide a perfect cavity structure for such resonance to occur. Here we report GaN-based microdisks with different diameters, based on a standard blue LED wafer on a Si substrate. A confocal photoluminescence spectroscopy is performed to analyze the properties of all microdisks. Then, we systematically study the effects of radial modes and axial modes of these microdisks on photon–electron coupling efficiency by using three-dimensional finite-difference time-domain simulations. For thick microdisks, photon–electron coupling efficiency is found to greatly depend on the distributions of both the radial modes and the axial modes, and the inclined sidewalls make significant influences on the axial mode distributions. These results are important for realization of high-efficiency resonant emission in GaN-based microcavity devices.

Keywords: microdisks, photon–electron coupling, whispering gallery mode, axial mode

PACS: 42.55.Sa, 42.60.Da **DOI:** 10.1088/1674-1056/ab9443

1. Introduction

The modulation of photons is an important field in semiconductor optoelectronics. The high-intensity photon distribution can be obtained from the highly localized light field in optical microcavities, which further induces strong photon–electron interactions. Optical microcavities have a variety of applications, such as light resonant emission, light transportation, light detection and light coupling.[1–4] Whispering gallery mode (WGM) optical microcavities, where the photon localization is formed by total internal reflection, have the highest optical feedback efficiency.[5]

GaN and its group-Ⅲ nitrides are typical wide bandgap semiconductor materials. The microdisks based on group-Ⅲ nitrides exhibit efficient blue-UV luminescence capability. In 2006, Choi *et al.* first fabricated GaN-based microdisks on Si substrates successfully.[6] The GaN-based microdisks, storing optical energy in the small cavity volume,[7] can provide low threshold, high quality (Q) factor and narrow resonance line width lasing.[8–10] In addition, the GaN-on-Si microdisks allow the formation of undercut structure by isotropic wet etching,[11,12] which makes the fabrication process simple and economical. The removal of Si substrates can form an atomically smooth bottom surface of the disk, which enhances the level of light field confinement of the microcavity. Moreover, the microdisks on Si substrates can be potentially used to integrate with Si electronics.

It is normally considered that the ideal microdisks should have the following characteristics: (1) the diameter must be small enough to reduce optical loss during the light propagation, and (2) the microdisks must be thin enough to concentrate the light field in the active region for high electron-photon coupling efficiency. However, the story seems different in the GaN-on-Si microdisks. In order to obtain high Q factor lasing, some researchers have been striving for ultra-small microdisks.[13,14] For ultra-small microdisks, the spatial spread of the optical modes into the surrounding beyond the physical boundaries results in low overlap between optical field and active region.[15] In addition, the radiation loss increases exponentially with the decreasing diameters.[16] As GaN-based materials are mostly obtained by heteroepitaxial growth, a large number of defects are generated at the epitaxial layer and substrate interface. The epitaxial layer must be thick enough to reduce the defect density, which is much larger than λ/n. Thus, the GaN-based microdisks are always

*Project supported by the National Key R&D Program of China (Grant Nos. 2016YFB0400102 and 2016YFB0400602), the National Natural Science Foundation of China (Grant Nos. 61674076, 61422401 and 51461135002), the Collaborative Innovation Center of Solid State Lighting and Energy-Saving Electronics, Open Fund of the State Key Laboratory on Integrated Optoelectronics (Grant No. IOSKL2017KF03), the Natural Science Foundation for Young Scientists of Jiangsu Province of China (Grant No. BK20160376), the Research Funds from NJU-Yangzhou Institute of Opto-electronics, and the Research and Development Funds from State Grid Shandong Electric Power Company and Electric Power Research Institute.

†Corresponding author. E-mail: pchen@nju.edu.cn

‡Corresponding author. E-mail: rzhang@nju.edu.cn

considered as thick disks. Conventional thin microdisks are relatively insensitive to axial dimension as the thickness of the microdisks is less than λ/n. In the case of the GaN-based microdisks, the influences of axial modes cannot be ignored. The influences of axial mode distributions on photon–electron coupling efficiency in thick GaN-based microdisks have not been investigated in detail, although thick microdisks are more suitable for the device working under electric injection in practical application.

In the present work, based on GaN-on-Si blue LED wafer, we fabricated circular microdisks with different diameters by photolithography and dry etching techniques. Scanning electron microscopy (SEM) was used to observe the morphology of microdisks, and confocal photoluminescence (PL) spectroscopy was performed to measure the optical properties of the microdisks. We systematically studied the influences of diameter and inclined sidewalls of the microdisks on electric field distributions and photon–electron coupling efficiency by three-dimensional finite-difference time-domain (3D-FDTD) simulations.

2. Experimental details

A standard GaN-on-Si blue LED wafer is used to fabricate the microdisks. The blue LED wafer consists of a 1.5 μm AlGaN buffer layer, a 1.5 μm n-GaN layer, 6 pairs of InGaN/GaN MQWs, and a 200 nm p-GaN layer. The total thickness is approximately 3.34 μm, which is one of the thickest microdisk structures. The diameters of the fabricated microdisks are 3.3 μm, 8 μm, and 18 μm, respectively. The use of standard LED epitaxial wafer provides convenience for electrically pumped lasing and commercial applications. The fabrication of the microdisks based on LED wafer has practical significance.

The fabrication procedure is as follows: Firstly, a 200 nm SiO_2 film is deposited by plasma enhanced chemical vapor deposition (PECVD), acting as a hard mask. Then, the SiO_2 film is patterned by photolithography. After that, RIE etching is used to etch the SiO_2 hard mask and ICP dry etching is used to form the disks. In order to obtain high quality microcavities, especially in terms of the smooth sidewall, we optimize the dry etching recipes to improve the etching morphology. The specific parameters are as follows: gas flow of Cl_2/BCl_3 is 48/6 sccm, RF/ICP power is 100/600 W, the chamber pressure is 10 mTorr. Finally, the sample is immersed in an HNO_3, HF and H_2O isotropic etchant to form the undercut structure.

Confocal Renishaw invia-reflex micro-photoluminescence (μ-PL) system is applied to measure the PL spectra of the microdisks. The laser beam is focused on surface of the microdisk through a microscope objective and the emission is collected by the same lens. The excitation source is a mode-locked Ti:sapphire pulsed laser with a pump wavelength of 375 nm, pulse width of 115 fs and repetition rate of 76 MHz. All measurements are performed at room temperature.

3. Results and discussion

The SEM images of the microdisks with different diameters are shown in Fig. 1. From Fig. 1, all microdisks show smooth morphology for outer surfaces, especially the sidewalls. Some surface contaminants can be seen in Fig. 1(b), which are residues from the final solution cleaning step. A large air gap between the microdisk and the Si substrate has been achieved by wet etching, which ensures that there is no damage to bottom surface of the microdisk. Due to the large air gap and smooth outer surface, the light can be effectively confined in the microdisk. A small inclination angle of the sidewalls of 2.5° from vertical can also be seen in all the samples. Obviously, the inclination angle plays an important role on the light confinement in the microdisk, which will be discussed in the last part of this paper. Thus, the smooth surface morphology and the undercut structure can support detailed and accurate study of the optical properties in GaN-based microdisks.

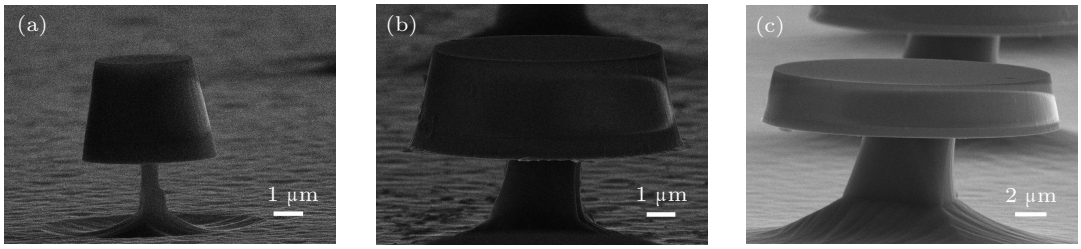

Fig. 1. Side-view SEM images of microdisks with the diameters of (a) 3.3 μm, (b) 8 μm, and (c) 18 μm.

The room-temperature PL spectra of 3.3 μm, 8 μm and 18 μm microdisks are shown in Fig. 2. It is well known that the effect of the surface defects is more serious at room temperature than that at low temperature, so the differences in room temperature PL are more obvious for the microdisks with different diameters. For all the samples, only the broad spontaneous emission spectra are observed at the lower pump power. When the pump power exceeds a threshold, clear and sharp peaks appear, although the broad spontaneous emission still gives a high background intensity. There is an obvious

blue shift of the spontaneous emission peak with the increase of pump power, which is the typical behavior of spontaneous emission. On the other hand, there is no shift in wavelength of these sharp peaks with the increase of pump power, which is the typical behavior of resonant emission. The integrated intensity verse pump power is plotted in Figs. 2(b), 2(d), and 2(f). All the curves show clear kinks, which confirms the transition from spontaneous radiation to resonant emission. The threshold is identified as the kink of the curve. The three microdisks show different thresholds: 0.085 mW for 3.3 μm microdisk, 3.581 mW for 8 μm microdisk, and 7.146 mW for 18 μm microdisks. The threshold increases with the increase of the diameter. Although the resonant peaks are unclear, the 3.3 μm microdisk has the lowest threshold as it has the smallest diameter. Comparing the three samples, the PL spectra of the 8 μm microdisk show the sharpest resonant emission peaks.

Next, 3D-FDTD is performed to study the electric field distributions of the 3.3 μm, 8 μm, and 18 μm microdisks. In the FDTD simulations, the distributions of the transverse electric (TE) modes are investigated. Radial electric field profiles of the dominant resonant peaks in the PL spectra of these three microdisks are shown in Fig. 3. The radial electric field profile at 443.7 nm of 3.3 μm microdisk is shown in Fig. 3(a). The radial mode is the first-order WGM in terms of radial mode number. The first-order WGM is confined along the edge of the microcavity, which shows high intensity in the outer 400 nm of the microcavity. The third-order WGM at 439.8 nm of the 8 μm microdisk is shown in Fig. 3(b). The 24th-order WGM at 446.1 nm of the 18 μm microdisk is shown in Fig. 3(c). This high-order WGM is concentrated near the center of the disk and shows a larger electric field distribution area.

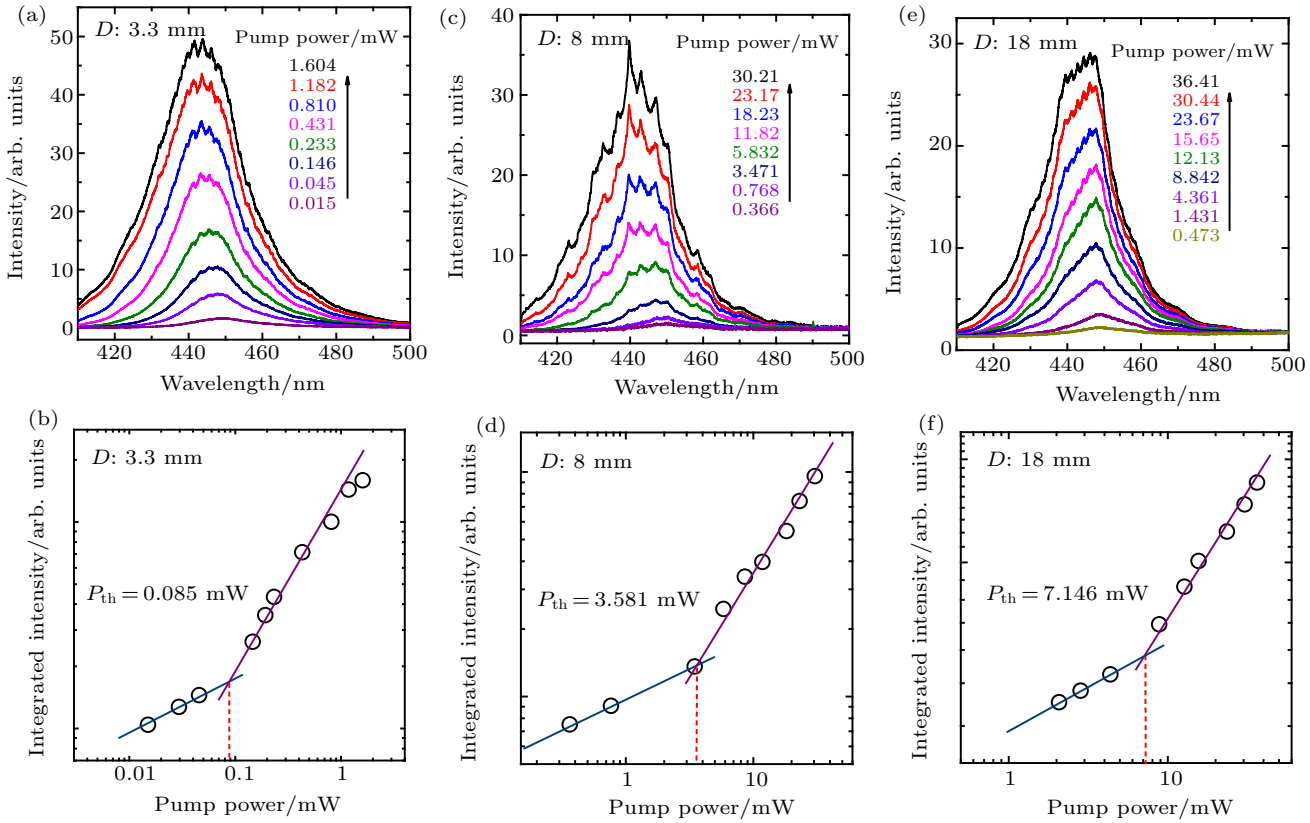

Fig. 2. Photoluminescence spectra of the microdisks with the diameters of (a) 3.3 μm, (c) 8 μm and (e) 18 μm with the increase of pump power at room temperature. Integrated PL intensity versus pump power for (b) 3.3 μm microdisk, (d) 8 μm microdisk and (f) 18 μm microdisk.

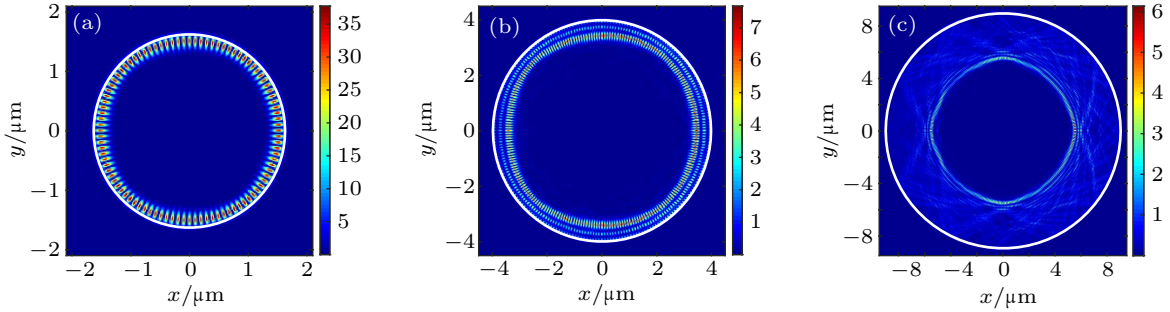

Fig. 3. Radial electric field profiles ($|E|^2$) of (a) 3.3 μm microdisk at 444 nm, (b) 8 μm microdisk at 440 nm and (c) 18 μm microdisk at 446 nm.

Normally, the first-order WGMs are preferentially excited by the pump power. However, the first-order WGMs in GaN-based microdisks are considered as high-loss modes.[14] GaN-based microdisks are usually fabricated by dry etching, which causes unavoidable surface damage and surface defects. The diffusion length of the electrons in GaN-based materials has been reported to be about 400 nm.[17,18] The carriers generated within 400 nm of the sidewalls have a high possibility of being captured by the surface defects before coupling with the first-order WGM. Thus, the first-order WGM at 443.7 nm in GaN-based microdisks has low photon–electron coupling efficiency. The 24th-order WGM in 18 μm microdisk is concentrated near the center of the disk, which may cause higher optical loss from the underlying post. Moreover, the larger distribution area of the electric field reduces the electric field intensity, which leads to lower photon–electron coupling efficiency. The third-order WGM is less affected by the sidewalls and underlying post. The relative small distribution area of the electric field increases the electric field intensity. Therefore the third-order WGM at 439.8 nm in 8 μm microdisk has higher photon–electron coupling efficiency and shows the sharpest resonant emission peak.

It should be noted that the thickness of the fabricated microdisks is much larger than λ/n, so the influence of axial mode on photon–electron coupling efficiency cannot be ignored. The axial electric field distributions of these thick microdisks with vertical sidewalls are simulated by 3D-FDTD. The axial electric field profiles of the 3.3 μm, 8 μm, and 18 μm microdisks are shown in Figs. 4(a)–4(c), respectively. The second-order standing-wave modes can be clearly discerned from the electric field profiles of 3.3 μm (Fig. 4(a)) and 18 μm (Fig. 4(c)) microdisks. The electric field profile of 8 μm microdisk (Fig. 4(b)) shows the third-order standing-wave mode. The axial modes have great effect on the coupling between active region and electric field. As shown in Fig. 4(b), the strongest intensity of electric field overlaps more with the MQWs, which is very important to obtain high-efficiency photon–electron coupling. The efficient photon–electron coupling further results in high-efficiency resonant emission. Therefore, the photon–electron coupling efficiency is affected by both radial modes and axial modes, which is completely different from the case of thin microdisks.

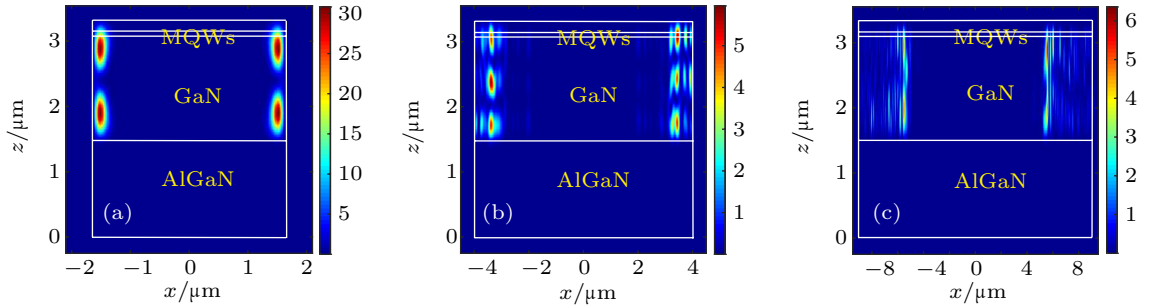

Fig. 4. Axial electric field profiles ($|E|^2$) of (a) 3.3 μm microdisk, (b) 8 μm microdisk, and (c) 18 μm microdisk with vertical sidawalls.

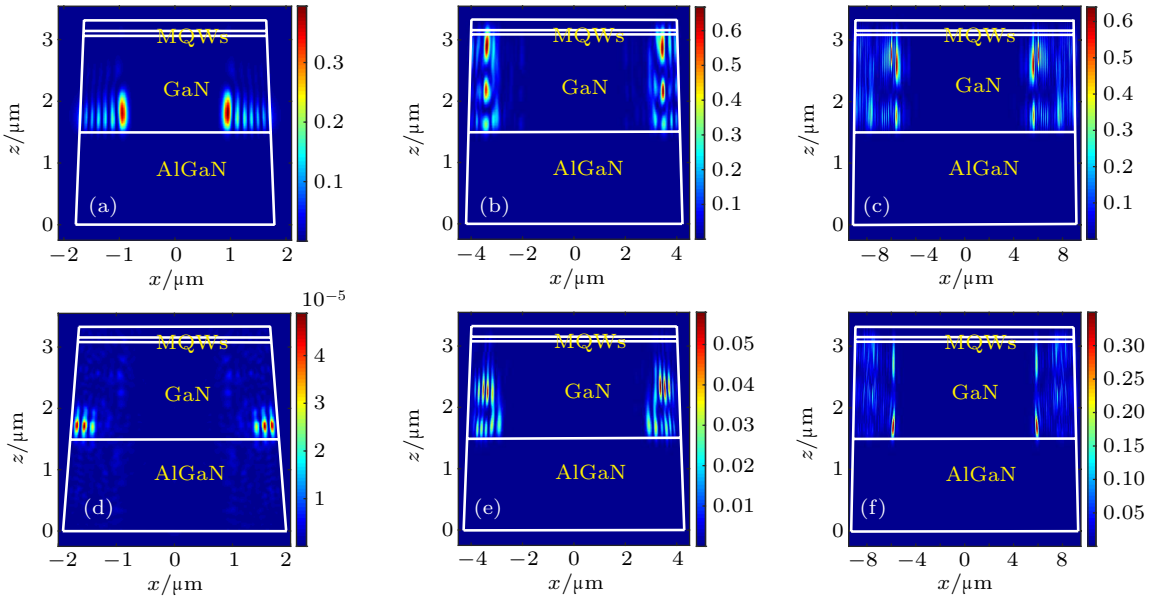

Fig. 5. Axial electric field profiles ($|E|^2$) of (a) 3.3 μm microdisk, (b) 8 μm microdisk, and (c)18 μm microdisk with inclination angles of 2.5°. Axial electric field profiles ($|E|^2$) of (d) 3.3 μm microdisk, (e) 8 μm microdisk, and (f) 18 μm microdiskwith inclination angles of 5°.

The SEM images of the fabricated microdisks show a small inclination angle of the sidewall of 2.5° from vertical. The inclined sidewalls are very common in thick microdisks, and the influences of the inclined sidewalls must be considered. Additional 3D-FDTD simulations have been performed on these three microdisks with inclination angles of 2.5° and 5°, and the axial electric field profiles are shown in Fig. 5. From the axial electric field profile of 3.3 μm microdisk with 2.5° inclination angle, it can be seen that the electric field is pronouncedly confined to the bottom of the n-GaN (Fig. 5(a)). This phenomenon is rather noticeable for the 3.3 μm microdisk with 5° inclination angles (Fig. 5(d)). For 8 μm (Fig. 5(b)) and 18 μm (Fig. 5(c)) microdisks with the inclination angle 2.5°, the inclined sidewalls make no significant effect on axial electric field distributions. As the inclination angle increases to 5°, the electric field is confined to the bottom of the n-GaN of the two microdisks (Figs. 5(e) and 5(f)). Moreover, the electric field intensity becomes weaker as the inclination angle increases. The inclined sidewalls confine the axial electric field to the bottom of the n-GaN and cause a lower coupling between MQWs and axial electric field. For thick microdisks with inclined sidewalls, the optical modes helically propagate upwards in the resonators. These helical modes have strong radial components, resulting in WGMs. These helical modes also have strong axial components, resulting in axial standing-wave modes. At a certain height, the smaller diameter on the upper part of the microdisk cuts off the net propagation of the mode in the axial direction and reflects it downwards.[19] Thus the axial modes are confined to the bottom of n-GaN. The larger the inclination angle, the shorter the axial propagation distance of the mode. Compared with 8 μm and 18 μm microdisks, the helical modes in 3.3 μm microdisk have weaker longitudinal wave-vector components. Thus the axial modes of 3.3 μm microdisk are less resonant.

Normally the microdisks with smaller diameter are considered as the promising candidates for resonant emission. However, the case is different for thick microdisks. According to Fig. 5(a), the axial electric field of the 3.3 μm microdisk with 2.5° inclination angle has little overlap with MQWs. Thus, the 3.3 μm microdisk has lower photon–electron coupling efficiency. This is another reason for the weaker resonant emission peaks in the PL spectra of the 3.3 μm microdisk. For the 8 μm microdisk with the 2.5° inclination angle, the axial electric field still overlaps with the MQWs. Thus, the 8 μm microdisk has higher photon–electron coupling efficiency and shows sharper resonant emission peak. Although the electric field distribution of 18 μm microdisk with 2.5° inclination angle is not affected by the inclined sidewalls, the higher-order WGM prevents the improvement of resonant efficiency.

4. Conclusions

In summary, the mode distributions and phto-pump emission spectra of GaN-based microdisks on Si have been systemically investigated. From the experimental results and theoretical calculations, three important rules can be concluded. Firstly, the photon–electron coupling efficiency in GaN-based microdisk is decided by both the radial modes and the axial modes. Secondly, the inclination angles of sidewalls make significant influences on the axial mode distributions. Thirdly, the GaN-based microdisks with small diameter (e.g., 3.3 μm) have lower photon–electron coupling efficiency because they are easier to be affected by surface defects and inclined sidewalls. The experimental results and simulated calculations clarify that there is an optimum GaN-based microdisks controlled by the diameter to obtain high-efficiency photon–electron coupling. WGM of the optimum microdisk should be confined in the region slightly away from the edge, not less than the carrier diffusion length. The axial electric field of the optimum microdisk is less affected by inclined sidewalls and has more overlap with the MQWs. In this work, the optimum disk diameter is 8 μm. We believe that our work provides a clear physical understanding to improve photon–electron coupling efficiency in GaN-based microdisks, which is of great significance in realizing high-efficiency GaN-based microcavity devices.

References

[1] Zhu J G, Ozdemir S K and Yang L 2014 *Appl. Phys. Lett.* **104** 171114
[2] Harker A, Mehrabani S and Armani A M 2013 *Opt. Lett.* **38** 3422
[3] Ma L B, Li S L, Fomin V M, Hentschel M, Gotte J B, Yin Y, Jorgensen M R and Schmidt O G 2016 *Nat. Commun.* **7** 10983
[4] Gambino S, Genco A, Accorsi G, Di Stefano O, Savasta S, Patane S, Gigli G and Mazzeo M 2015 *Appl. Mater. Today* **1** 33
[5] He L N, Ozdemir S K and Yang L 2013 *Laser Photon. Rev.* **7** 60
[6] Choi H W, Hui K N, Lai P T, Chen P, Zhang X H, Tripathy S, Teng J H and Chua S J 2006 *Appl. Phys. Lett.* **89** 211101
[7] Yang Y D, Tang M, Wang F L, Xiao Z X, Xiao J L and Huang Y Z 2019 *Photon. Res.* **7** 594
[8] Feng M X, He J L, Sun Q, Gao H W, Li Z C, Zhou Y, Liu J P, Zhang S M, Li D Y, Zhang L Q, Sun X J, Li D B, Wang H B, Ikeda M, Wang R X and Yang H 2018 *Opt. Express* **26** 5043
[9] Aharonovich I, Woolf A, Russell K J, Zhu T T, Niu N, Kappers M J, Oliver R A and Hu E L 2013 *Appl. Phys. Lett.* **103** 021112
[10] Yuan G, Zhang C, Xiong K L and Han J 2018 *Opt. Lett.* **43** 5567
[11] Zhu G Y, Li J P, Li J T, Guo J Y, Dai J, Xu C X and Wang Y J 2018 *Opt. Lett.* **43** 647
[12] Zhang Y Y, Ma Z T, Zhang X H, Wang T and Choi H W 2014 *Appl. Phys. Lett.* **104** 221106
[13] Athanasiou M, Smith R, Liu B and Wang T 2015 *Sci. Rep.* **4** 7250
[14] Tamboli A C, Haberer E D, Sharma R, Lee K H, Nakamura S and Hu E L 2007 *Nat. Photon.* **1** 61
[15] Nezhad M P, Simic A, Bondarenko O, Slutsky B, Mizrahi A, Feng L A, Lomakin V and Fainman Y 2010 *Nat. Photon.* **4** 395
[16] Bogdanov A A, Mukhin I S, Kryzhanovskaya N V, Maximov M V, Sadrieva Z F, Kulagina M M, Zadiranov Y M, Lipovskii A A, Moiseev E I, Kudashova Y V and Zhukov A E 2015 *Opt. Lett.* **40** 4022
[17] Yakimov E B, Vergeles P S, Polyakov A Y, Smirnov N B, Govorkov A V, Lee I H, Lee C R and Pearton S J 2007 *Appl. Phys. Lett.* **90** 152114
[18] Hafiz S, Zhang F, Monavarian M, Avrutin V, Morkoc H, Ozgur U, Metzner S, Bertram F, Christen J and Gil B 2015 *J. Appl. Phys.* **117** 013106
[19] Chen R, Tran T T D, Ng K W, Ko W S, Chuang L C Sedgwick F G and Chang-Hasnain C 2011 *Nat. Photon.* **5** 170